Inorganic Chemistry

pubs.acs.org/IC Article

Dimensionality Control of 1D Coupling Reaction for the Facile Preparation of Porous Carbon Nanofibers

Zhuojun Yan, Bo Cui, Na Li, Dongqi Yang, Jialin Xie, Tongfei Geng, Yimin Qiao, Yi Jiang, Naishun Bu,* Ye Yuan,* and Lixin Xia*

Cite This: *Inorg. Chem.* 2021, 60, 18058−18064 Read Online

ACCESS | Metrics & More | Article Recommendations | Supporting Information

ABSTRACT: Porous carbon nanofibers with unique hierarchical structures have great potential in many fields, including heterogeneous catalysis, optoelectronics, and sensing. However, several preparation issues, such as additional templates, complicated processes, and harsh conditions, seriously hamper their widespread use. Here, we control the Sonogashira coupling reaction of linear building monomers—1,4-dibromaphthalene and 1,4-ethylbenzene—at the molecular level. Due to the occurrence of branching chain reaction (side reaction), 1D oligomer expands the growth orientation in the plane direction, forming a curled 1D fiber polymer. After thermal-driven skeleton engineering, porous carbon nanofibers were obtained with hierarchical channels of macro- (150 nm), meso- (5.2 nm), and microcavities (0.5 and 1.3 nm). The integration of macro-/meso-/microporous structure reveals a fast and sufficient interaction with electrolyte molecules, facilitating the construction of high-performance electrical devices. Our strategy, using a side reaction to achieve the dimensionality control of 1D copolymerization, paves a new way for the facile preparation of porous carbon nanofibers.

1. INTRODUCTION

Porous carbon nanotubes (CNT) have been the subject of much interest in recent years due to their large surface area, high porosity, and high-density active sites.[1] Porous carbon nanofibers (CNF) are 1D nanomaterials with a structure more complicated than the one of carbon nanotubes (CNT).[2] Based on their unique hierarchical structure, hollow CNF solids are characterized by open channels for the fast transfer of external substrates and sufficient contact area for their full interaction, holding great promise for many applications, including heterogeneous catalysis, optoelectronics, and sensing.[3,4] Current efforts are devoted to anatomizing the techniques of CNF preparation and fabrication as well as on further exploring their applications.[5,6] Unfortunately, the widespread utilization of CNF is seriously hampered by some preparation issues, such as limited methods (biomass methods, laser ablation, vapor deposition), complicated processes (additional template/inducers), and harsh conditions (pressure, temperature, electrification).[7−10] Therefore, a template-free, facile approach is considered a great challenge to obtain 1D porous carbon nanofibers in a large amount.[11]

Porous polymers are considered a new generation of functional porous solids due to the synthetic diversity, large surface area, and high porosity. During the past decades, a broader variety of microporous polymers, such as covalent organic frameworks (COFs), polymers of intrinsic microporosity (PIMs), conjugated microporous polymers (CMPs), and porous aromatic frameworks (PAFs), have been reported under the guidance of the rigid node-strut topology and cross-coupling chemistry.[12−16] Most polymers precipitate as irregular or spherical solids with submicrometer dimensions; under a bias, the external surfaces accumulated with abundant charged species inhibit the transfer/transport of electrolytes inside particle due to the electrostatic repulsion, leading to the high diffusion resistance of ionic guests.[17] Based on the structural tunability, facile preparation of porous polymer-based carbon nanofibers that integrate low ion diffusion resistance and high electronic conductivity brings about significant breakthroughs and new synthetic concepts for the development of advanced electrochemical materials.

In this study, 1,4-dibromaphthalene and 1,4-ethylbenzene serving as linear building units are cross-linked through Sonogashira−Hagihara coupling reaction. Because of the cyclotrimerization of alkynyl groups, we observed a remarkably selective formation of 1D polymeric tubes because of the

Received: August 29, 2021
Published: November 11, 2021

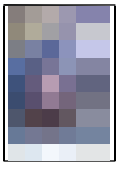

https://doi.org/10.1021/acs.inorgchem.1c02673
Inorg. Chem. 2021, 60, 18058−18064

Figure 1. (a) Main reaction and (b) side reaction of Sonogashira–Hagihara coupling. (c) Synthesis of LNU-8 polymer.

Figure 2. (a,b) FTIR spectra of 1,4-diethynylbenzene, 1,4-dibromonaphthalene, and LNU-8 polymer. (c) Solid-state ^{13}C NMR spectrum of LUN-8 polymer and (d) N_2 adsorption–desorption isotherms and pore size distributions of LNU-8 and LNU-8-900, respectively.

concentration effect of monomers.[18] Through high-temperature carbonization of the as-formed tubular polymers, porous carbon nanofibers were obtained with a surface area up to 684 $m^2\ g^{-1}$, an average outer diameter of ~400 nm, and channel width of ~150 nm. As an electrode, the resulting porous carbon nanofibers manifested the strong relationship between morphology and performance (nanofiber > bulk), and the interfacial charge-transfer resistance reached the lowest level with a value of 0.45 Ω. Thereby, a template-free synthesis of porous carbon nanofibers was achieved, which provides a new insight into high-performance electrochemical materials.

2. EXPERIMENTAL SECTION

2.1. Materials. 1,4-Dibromonaphthalene was purchased from J&K chemical and 1,4-diethynylbenzene was received from TCI. Copper iodide and tetrakis(triphenylphophine)palladium were obtained from Sigma-Aldrich. Other chemicals and solvents were purchased from commercial suppliers and used without further purification. All reactions were performed under a purified nitrogen atmosphere.

2.2. Synthesis of LNU-8. 1,4-Dibromonaphthalene (1.584 mmol, 453 mg), 1,4-ethynylbenzene (1.980 mmol, 250 mg), tetrakis-(triphenylphosphine)palladium (30 mg), and copper(I) iodide (10 mg) were added into a round-bottom flask. The mixture was degassed through a N_2 bubbling process for 30 min; after that, 10 mL of anhydrous *N*,*N*′-dimethylformamide (DMF) and 8 mL of anhydrous triethylamine (TEA) were added into the system. Then, the reaction mixture was heated to 80 °C for 72 h under N_2 gas atmosphere.

https://doi.org/10.1021/acs.inorgchem.1c02673
Inorg. Chem. 2021, 60, 18058–18064

Figure 3. (a,b) Powder X-ray diffraction patterns of fibers LNU-8 carbons and bulk LNU-B carbons. (c) TGA plots of LNU-8 and LNU-B at N_2 condition with a ramp rate of 5 °C min^{-1}. (d) Raman spectrum of fibers LNU-8 carbons and bulk LNU-B carbons.

Cooling to room temperature, the precipitate was filtered and purified by Soxhlet extraction using each tetrahydrofuran, ethanol, and chloroform for 24 h. Finally, the yellow-brown sample LNU-8 was obtained by drying at 90 °C for 10 h under vacuum.

2.3. Synthesis of LNU-8 Porous Carbon Nanofibers. LNU-8 powder was heated in a furnace tube at a ramp rate of 2 °C min^{-1} to the target temperature (800, 900, and 950 °C) in a high pure nitrogen atmosphere and held for 60 min to produce carbonized LNU-8 porous carbon nanotubes, denoted as LNU-8-800, LNU-8-900, and LNU-8-950.

2.4. Electrochemical Characterization. Electrochemical measurements were conducted on an electrochemical workstation (CHI 660E). A standard three-electrode configuration was used throughout this study. Working electrode was prepared by the dropping method.[19−22] Briefly, 5 mg of as-prepared carbonized LNU solid was dispersed in 1 mL of 0.05 wt % Nafion solution by ultrasonification for 30 min. The modified glassy carbon electrode was made by dropping 25 μL (0.125 mg) of the dispersion on glassy carbon (GC: 3 mm diameter) and drying the glassy carbon at 60 °C overnight. A platinum foil was applied as a counter electrode with a standard Ag/AgCl reference electrode. H_2SO_4 aqueous solution (1 M) was used as the electrolytic solution. The electrochemical properties were investigated using the cyclic voltammogram (CV), galvanostatic charge−discharge curve, and Nyquist plot. The operating voltage ranged from 0 to 0.8 V for galvanostatic charge−discharge and cyclic voltammograms tests. The specific capacitance was calculated by cyclic voltammetry using eq 1:[23,24]

$$C = \frac{1}{ms(V_f - V_i)} \int_{V_i}^{V_f} I(V)\mathrm{d}V \quad (1)$$

where m is the loading mass of electrode materials and s is the scan rate, V_f and V_i are the integration limits of the voltametric curve, and $I(V)$ is the response current density.

3. RESULTS AND DISCUSSION

1,4-Dibromonaphthalene and 1,4-diethynylbenzene form a 1D polymer under conventional Sonogashira coupling conditions (Figure 1a). Due to the self-coupling effect of 1,4-diethynylbenzene, 1D oligomer expands the growth orientation in the plane direction, forming the curled 1D fiber polymer (Figure 1b,c).[18] As illustrated in Fourier transform infrared spectroscopy (FTIR) spectra (Figure 2a), the C-Br stretching vibration of 1,4-dibromonaphthalene at 970 cm^{-1} and the C−H stretching vibration of the terminal alkyne (1,4-acetylbenzene) at 3270 cm^{-1} disappear from IR spectrum of LNU-8, verifying the completeness of the Sonogashira−Hagihara coupling reaction. Apart from the deformation vibration of the disubstituted naphthalene ring (770−760 cm^{-1}) and the disubstituted benzene ring (835−825 cm^{-1}), there is an emerging peak ascribed to the deformation vibration of trisubstituted benzene ring centered at ∼790 cm^{-1}, which indicates the occurrence of the side reaction derived from the alkynyl groups (Figure 2b).

This result is confirmed by the solid-state ^{13}C CP/MAS NMR spectrum of LNU-8 polymer (Figure 2c). A series of peaks observed at 120−150 ppm is attributed to the aromatic carbons, and the signals at 95.3 and 83.5 ppm correspond to the alkyne carbons. Correspondingly, the experimental ratio of the integral area for the alkyne carbons to that for the aromatic carbons is ca. 9.35%. This value is much lower than the theoretical amount (20%), which is consistent with the conclusion obtained from the above FTIR spectra that the cyclotrimerization of alkynes into trisubstituted benzene ring.[25]

As shown in Figure S1, no obvious sharp peaks were observed in the powder X-ray diffraction spectrum (PXRD) before carbonization of the polymer, indicating that the

https://doi.org/10.1021/acs.inorgchem.1c02673
Inorg. Chem. 2021, 60, 18058−18064

obtained material is amorphous. As shown in Figure 3a,b, LNU-8 porous carbon nanofibers have two broad peaks at 23° and 43°, corresponding to the (002) and (100) crystal planes of the porous carbon material, respectively. These two characteristic peaks indicate that the carbonized material has a certain degree of graphitization.[26] Thermogravimetric analysis (TGA) illustrates a ca. 3.40% weight loss before 370 °C, corresponding to the escape of solvent and oligomer molecules (Figure 3c). After that, there is 9.09% weight loss in the range of 370−680 °C ascribed to the C−H bond fracture and thermal curing of aromatic rings, indicating a quite high carbonization yield.[27] At the same time, the high carbonization yield of LNU-8 compared with LNU-B is ascribed to the effect of acetylene moieties which are thermally polymerized and enhance the carbonization yield.[28−31] Finally, the thermal-driven skeleton engineering (700−900 °C) results in the formation of micro- and mesopores.[32] These transformations are confirmed by the Raman spectra (Figure 3d). All carbonized materials have two distinct characteristic peaks at about 1350 cm^{-1} (D-band) and 1590 cm^{-1} (G-band) showing the formation of defects and graphitic fragments. The I_D/I_G ratio for the carbonized solids ranged from 0.83 (LNU-8-800) to 1.01 (LNU-8-950) demonstrates the increased degree of graphitization.

The evolution of pore structure with increasing carbonization temperature was analyzed from the N_2 adsorption−desorption isotherms (Figures 2d and S2). According to the N_2 isotherms, the BET surface area of LNU-8 is calculated to be 43 m^2 g^{-1} in the range of P/P_0 = 0.03−0.25. Due to the low content of side reactions, most of the building monomers are cross-linked along the direction of the polymer backbone. The close-packed structure of the $\pi-\pi$ interaction results in a low BET surface area of LNU-8. Carbonized solids (LNU-8-800 and LNU-8-950) show a type I gas sorption isotherm with high nitrogen gas adsorption at low relative pressure (P/P_0 < 0.05), suggesting the presence of abundant micropores within the carbon nanofibers. LNU-8-900 shows a type IV isotherm with a slight sorption hysteresis in the range of P/P_0 ∼ 0.5−1.0, proving the mesoporous of LNU-8-900 porous network. After carbonizing at a high-temperature, the resulting porous carbon nanofibers possess high surface areas of 361 m^2 g^{-1} for LNU-8-800, 684 m^2 g^{-1} for LNU-8-900, and 312 m^2 g^{-1} for LNU-8-950, respectively (Table S1). The surface area of LNU-8-900 is much higher than that of much the reported 1D porous carbon materials, including CF-CNT-1 (565 m^2 g^{-1}),[33] N-CNTs (192 m^2 g^{-1}),[34] and N-CNT1 (200 m^2 g^{-1}).[35] Figure 2d shows the pore size distributions calculated using a density functional theory (DFT) model. The pore size of LNU-8-900 was mainly concentrated at 0.5, 5.2, and 1.3 nm, respectively. This unique micro- and mesoporous structure is beneficial to increase the accessible surface area and the diffusion rate of electrolyte ions according to the "oscillation theory."[36] When the carbonization temperature increases from 800 to 950 °C, excessive carbonization causes structural collapse and reduced surface area. Especially for 950 °C, a higher carbonization temperature causes significant skeleton shrinkage and a decrease in surface area. Therefore, 900 °C is a preferred and optimized temperature for the carbonization of LNU-8 into porous carbon nanofibers, resulting in high surface area. A similar trend is also observed for LNU-B samples (Figure S3).

Scanning electron microscopy (SEM) image shows that LNU-8 mainly exists in the form of 1D polymeric tubes, with an average outer diameter ∼400 nm and several microns in length (Figure 4a). This is due to the concentration effect of raw monomers, the 2D planar structures tend to roll up or

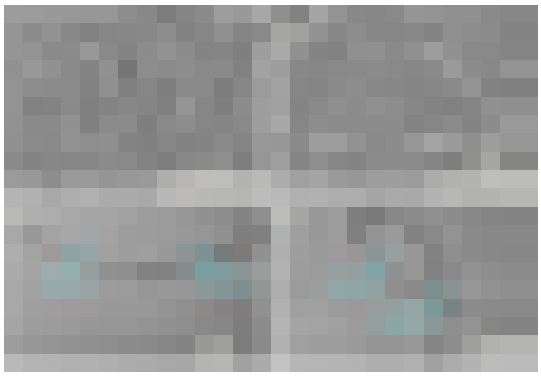

Figure 4. SEM and TEM images of LNU-8 (a,c) and LNU-8-900 (b,d), respectively.

closely connect to form a 1D cylindrical geometry.[18] As illustrated in transmission electron microscopy (TEM) image (Figures 4c and S4), LNU-8 polymer adopts a hollow structure with an average outer diameter of ∼400 nm, channel width of ∼90 nm. After carbonization, there is no obvious change in appearance and diameter for the porous carbon nanofibers (Figure 4b). TEM image revealed that LNU-8-900 solid exists as nanofibers with a mean exterior diameter of 400 nm and inner diameter ∼150 nm (Figure 4d). The shrinkage of wall thickness is attributed to the structure engineering of LNU-8 skeleton, enlarging the interior pore channels.

To manifest the concentration effect, we changed the concentration (two-thirds of the original concentration of LNU-8) of the reactants and prepared the polymer sample in bulk morphology, named LNU-B (Table S2). SEM images show that the obtained LNU-B solid is composed of fused polymer masses without well-defined shape (Figure S5). LNU-B also reveals a low BET surface area with a value of 29 m^2 g^{-1} and uniform pore size distribution ∼1.5 nm (Figure S3). Similarly, the LNU-B bulk carbons (LNU-B-800, LNU-B-900, and LNU-B-950) were prepared through high-temperature carbonization (Figure S5). The resulting porous carbons possess high surface areas of 165.9 m^2 g^{-1} for LNU-B-800, 644.9 m^2 g^{-1} for LNU-B-900, and 349.9 m^2 g^{-1} for LNU-B-950 (Table S1). Pore size distribution analysis from the adsorption isotherms indicated that all carbonized solids possess only a microporous structure with a pore size distribution in the range of 0.5−1.5 nm.

The electrochemical properties of LNU-derived samples were investigated in a 1 M H_2SO_4 aqueous electrolyte using a three-electrode cell system, in which Pt wire was used as the counter electrode and a standard Ag/AgCl electrode as a reference electrode. As illustrated in Figure 5a, the specific area calculated from the cyclic voltammogram (CV) curve at 10 mV s^{-1} for LNU-8-900 is apparently larger than that of LNU-8-800 and LNU-8-950, due to its large ion-accessible surface area and rational porous structure. Galvanostatic charge−discharge (GCD) measurement reveals the largest specific capacitance of LNU-8-900 consistent with the CV conclusion (Figure 5b). Examined at different scan rates (Figure 5c), all cyclic voltammogram curves for LNU-8-900 sample kept the "rectangular shape" even at a potential scan rate of 200 mV s^{-1}, indicating a nearly ideal electrical double-layer capacitive behavior and efficient transport of electrolyte ions.[37] The initial

https://doi.org/10.1021/acs.inorgchem.1c02673
Inorg. Chem. 2021, 60, 18058−18064

Figure 5. (a) Cyclic voltammograms of fibers LNU-8 carbons at a scan rate of 10 mV s^{-1}. (b) GCD curves of fibers LNU-8 carbons at 1 A g^{-1}. (c) Cyclic voltammograms of LNU-8-900 at different scan rates in 1 M H_2SO_4 solution. (d) GCD curves of LNU-8-900 at different current densities. (e) Cyclic voltammograms of LNU-B-900 at different scan rates in 1 M H_2SO_4 solution. (f) GCD curves of LNU-B-900 at different current densities.

specific capacitance for LNU-8-900 was 285 F g^{-1} at a scan rate of 2 mV s^{-1}, which remained 78% (221 F g^{-1}) at a higher scan rate of 50 mV s^{-1}. On the contrary, the initial specific capacitance for LNU-B-900 is only 245 F g^{-1} at a scan rate of 2 mV s^{-1} and the value decreases to 104 F g^{-1} at a higher scan rate of 50 mV s^{-1} (Figure 5e), which is much lower than those of LNU-8-900 at the same conditions. This higher performance of LNU-8-900 compared with that of LNU-B-900 is ascribed to the meso- and macroporous channels provide a continuous diffusion path for exchanging guest electrolytes with the exterior, and the microporous cavities generate sufficient contact area for full interaction. Notably, the specific capacitance for LNU-8-900 approaches the highest level among the pure carbon-based electrodes including carbonization of HG-CNT-HCNO (236.5 F g^{-1} at 0.5 A g^{-1}),[38] PAF-1 (146 F g^{-1} at 1 A g^{-1}),[39] self-template strategy (206 F g^{-1} g at 1 A g^{-1}),[40] carbonization of covalent benzoxazine framework (185 F g^{-1} at 1 A g^{-1}),[41] template-assisted strategy (268 F g^{-1} at 0.25 A g^{-1}),[42] and carbonization of nanoparticles (206 F g^{-1} at 1 A g^{-1})[43] (Table S3).

As shown in Figure 5d, it is clear that the charge and discharge curves at current densities ranged from 0.2 to 5 A g^{-1} present a semi-triangular shape with high reversibility. There is no obvious shoulder peak observed in charge−discharge curve, indicating the double-layer mechanism for LNU-8-900 instead of the pseudocapacitance process. The constant current charge−discharge curve of LNU-8-900 shows good triangular symmetry, indicating that LNU-8-900 has a higher Coulombic efficiency as an electrode material. It is attributed to the shuttle effect resulting from the relatively lower surface area and higher microporosity, which traps the electrode ions leading to the decreased speed of charge transfer.[44] The longer duration time for discharge process than charge time manifests that LNU-8-900 electrode has good conductivity and no obvious polarization. The stability of LNU-8-900 was tested using cycling experiments at a sweep of 10 mV s^{-1}. As depicted in Figure S6, LNU-8-900 showed little capacitance decay (8.5% for LNU-8-900) after 5000 cycles.

Electrochemical impedance spectroscopy (EIS) measurement was also conducted to reveal the resistance and the electrical conductivity behavior of LNU-8-900 electrode (Figure 6). The Nyquist plot shows a tiny semicircle at high

Figure 6. Nyquist plot at a high frequency with the inset showing the possible mechanism for the diffusion of electrolytes.

frequencies, of which the radius represents R_{ct} and a linear curve at low frequencies. With similar specific surface area (684 m^2 g^{-1} for LNU-8-900 and 644.9 m^2 g^{-1} for LNU-B-900), but different morphologies (tubular for LNU-8-900 and bulk for LNU-B-900), the R_{ct} value of LNU-8-900 is 0.45 Ω calculated by the equivalent circuit, which is one-third of the resistance of the block sample LNU-B-900 (Figure S7). This phenomenon is due to the integration of micro-, meso-, and macroporous structure of LNU-8-900 provides short and effective electrolyte

https://doi.org/10.1021/acs.inorgchem.1c02673
Inorg. Chem. 2021, 60, 18058−18064

transport pathways, leading to low resistance for charge/ion transfer.

4. CONCLUSIONS

Based on the side reaction of Sonogashira−Hagihara coupling, we synthesized a 1D tubular polymer using linear building monomers without any template and surfactant. High-quality porous carbon nanofibers were then obtained by direct carbonization of the tubular polymer precursor. The resulting solid shows a high surface area and hierarchical channels. The combination of macro-/meso-channels and numerous micro-porous cavities in the hollow porous nanofibers enables a rapid transfer and full contact for electrolytes, thus endowing an ultralow interfacial charge-transfer resistance. This study provides an ideological guidance for the realization of the tubular morphological engineering and broadens the scope of their potential application in sensing, catalysis, photoelectricity, and energy storage fields.

■ ASSOCIATED CONTENT

Supporting Information

The Supporting Information is available free of charge at https://pubs.acs.org/doi/10.1021/acs.inorgchem.1c02673.

Supporting Information is obtained free of charge on ACS Publications website at XRD pattern, Cumulative pore volume curves, SEM and TEM images, Cycle life test, Nyquist plots, Porosity parameters, Comparison with reported works (PDF)

■ AUTHOR INFORMATION

Corresponding Authors

Naishun Bu − *School of Environmental Science, Liaoning University, Shenyang 110036, P. R. China;* orcid.org/0000-0002-3987-2661; Email: bunaishun@lnu.edu.cn

Ye Yuan − *Key Laboratory of Polyoxometalate and Reticular Material Chemistry of Ministry of Education, Faculty of Chemistry, Northeast Normal University, Changchun 130024, P. R. China;* orcid.org/0000-0002-0298-2023; Email: Yuany101@nenu.edu.cn

Lixin Xia − *College of Chemistry, Liaoning University, Shenyang 110036, P. R. China; Liaoning Key Laboratory of Chemical Additive Synthesis and Separation, Yingkou Institute of Technology, Yingkou 115014, P. R. China;* Email: lixinxia@lnu.edu.cn

Authors

Zhuojun Yan − *College of Chemistry, Liaoning University, Shenyang 110036, P. R. China*

Bo Cui − *College of Chemistry, Liaoning University, Shenyang 110036, P. R. China*

Na Li − *College of Chemistry, Liaoning University, Shenyang 110036, P. R. China*

Dongqi Yang − *College of Chemistry, Liaoning University, Shenyang 110036, P. R. China*

Jialin Xie − *College of Chemistry, Liaoning University, Shenyang 110036, P. R. China*

Tongfei Geng − *College of Chemistry, Liaoning University, Shenyang 110036, P. R. China*

Yimin Qiao − *College of Chemistry, Liaoning University, Shenyang 110036, P. R. China*

Yi Jiang − *College of Chemistry, Liaoning University, Shenyang 110036, P. R. China;* orcid.org/0000-0002-6266-7615

Complete contact information is available at: https://pubs.acs.org/10.1021/acs.inorgchem.1c02673

Author Contributions

The manuscript was written through contributions of all authors. All authors have given approval to the final version of the manuscript.

Notes

The authors declare no competing financial interest.

■ ACKNOWLEDGMENTS

We gratefully acknowledge the supports from the National Natural Science Foundation of China (31972522, 21704037, 21671089), National Key Research and Development Project of China (2018YFC1801200), Major Science and Technology Project of Liaoning Province (2019JH1/10300001), the Scientific Research Fund of Liaoning Provincial Education Department (2020-YKLH-22), Liaoning Revitalization Talents Program (XLYC2007032, XLYC1807210), Scientific Research Fund of Liaoning Provincial Education Department (LQN202003).

■ REFERENCES

(1) Wang, X. Y.; Mu, P.; Zhang, C.; Chen, Y.; Zeng, J. H.; Wang, F.; Jiang, J. X. Control Synthesis of Tubular Hyper-Cross-Linked Polymers for Highly Porous Carbon Nanotubes. *ACS Appl. Mater. Interfaces* **2017**, *9*, 20779−20786.

(2) Yadava, D.; Amini, F.; Ehrmann, A. Recent Advances in Carbon Nanofibers and Their Applications − A Review. *Eur. Poly. J.* **2020**, *138*, 109963−109976.

(3) Bi, Z. H.; Kong, Q. Q.; Cao, Y. F.; Sun, G. H.; Su, F. Y.; Wei, X. X.; Ahmad, A.; Chen, C. M. Biomass-Derived Porous Carbon Materials with Different Dimensions for Supercapacitor Electrodes: A Review. *J. Mater. Chem. A* **2019**, *7*, 16028−16045.

(4) Zhou, W. J.; Liu, H.; Boughton, R. I.; Du, G. J.; Lin, J. J.; Wang, J. Y.; Liu, D. One-Dimensional Single-Crystalline Ti-O Based Nanostructures: Properties, Synthesis Modifications and Applications. *J. Mater. Chem.* **2010**, *20*, 5993−6008.

(5) Li, W. H.; Li, M. S.; Adair, K. R.; Sun, X. L.; Yu, Y. Carbon Nanofiber-Based Nanostructures for Lithium-Ion and Sodium-Ion Batteries. *J. Mater. Chem. A* **2017**, *5*, 13882−13906.

(6) Gawel, K.; Wenner, S.; Edvardsen, L. Effect of Carbonation on Bulk Resistivity of Cement/Carbon Nanofiber Composites. *Constr. Build. Mater.* **2021**, *305*, 124794−124804.

(7) Zhang, X. Q.; Sun, Q.; Dong, W.; Li, D.; Lu, A. H.; Mu, J. Q.; Li, W. C. Synthesis of Superior Carbon Nanofibers with Large Aspect Ratio and Tunable Porosity for Electrochemical Energy Storage. *J. Mater. Chem. A* **2013**, *1*, 9449−9455.

(8) Hou, H. S.; Jing, M. J.; Yang, Y. C.; Zhang, Y.; Song, W. X.; Yang, X. M.; Chen, J.; Chen, Q. Y.; Ji, X. B. Antimony Nanoparticles Anchored on Interconnected Carbon Nanofibers Networks as Advanced Anode Material for Sodium-Ion Batteries. *J. Power Sources* **2015**, *284*, 227−235.

(9) Li, W. H.; Zeng, L. C.; Wu, Y.; Yu, Y. Nanostructured Electrode Materials for Lithium-Ion and Sodium-Ion Batteries via Electrospinning. *Sci. China Mater.* **2016**, *59*, 287−321.

(10) Zheng, G. Y.; Zhang, Q. F.; Cha, J. J.; Yang, Y.; Li, W. Y.; Seh, Z. W.; Cui, Y. Amphiphilic Surface Modification of Hollow Carbon Nanofibers for Improved Cycle Life of Lithium Sulfur Batteries. *Nano Lett.* **2013**, *13*, 1265−1270.

(11) Li, J.; Zhou, Y. N.; Xiao, X.; Wang, W.; Wang, N.; Qian, W. Z.; Chu, W. Regulation of Ni-CNT Interaction on Mn-Promoted Nickel Nanocatalysts Supported on Oxygenated CNTs for CO_2 Selective Hydrogenation. *ACS Appl. Mater. Interfaces* **2018**, *10*, 41224−41236.

(12) Yue, J. Y.; Wang, L.; Ma, Y.; Yang, P.; Zhang, Y. Q.; Jiang, Y.; Tang, B. Metal Ion-Assisted Carboxyl-Containing Covalent Organic

Frameworks for the Efficient Removal of Congo Red. *Dalton Trans.* **2019**, *48*, 17763−17769.
(13) Li, F.; Wang, D. K.; Xing, Q. J.; Zhou, G.; Liu, S. S.; Li, Y.; Zheng, L. L.; Ye, P.; Zou, J. P. Design and Syntheses of MOF/COF Hybrid Materials via Postsynthetic Covalent Modification: An Efficient Strategy to Boost the Visible-Light-Driven Photocatalytic Performance. *Appl. Catal., B* **2019**, *243*, 621−628.
(14) Zhang, Y. M.; Hu, Y. M.; Zhao, J. H.; Park, E.; Jin, Y. H.; Liu, Q. J.; Zhang, W. Covalent Organic Framework-Supported Fe-TiO_2 Nanoparticles as Ambient-Light-Active Photocatalysts. *J. Mater. Chem. A* **2019**, *7*, 16364−16371.
(15) Xu, J. W.; Ou, J. J.; Chen, L. F.; Zhang, H. Y.; Ma, S. J.; Ye, M. L. Palladium Catalyst Imbedded in Polymers of Intrinsic Microporosity for the Suzuki-Miyaura Coupling Reaction. *RSC Adv.* **2018**, *8*, 35205−35210.
(16) Priyanka; Kumar, A. Multistimulus-Responsive Supramolecular Hydrogels Derived by in Situ Coating of Ag Nanoparticles on 5′-CMP-Capped β-FeOOH Binary Nanohybrids with Multifunctional Features and Applications. *ACS Omega* **2020**, *5*, 13672−13684.
(17) Brukhno, A. V.; Akinshina, A.; Coldrick, Z.; Nelsona, A.; Auer, S. Phase Phenomena in Supported Lipid Films under Varying Electric Potential. *Soft Matter* **2011**, *7*, 1006−1017.
(18) Chun, J. J.; Park, H.; Kim, J.; Lee, S. M.; Kim, H. J.; Son, S. U. Tubular-Shape Evolution of Microporous Organic Networks. *Chem. Mater.* **2012**, *24*, 3458−3463.
(19) Chen, J.; Li, C.; Lian, Y.; Chen, Y.; Chen, T.; Hu, X. Understanding the Oxygen-Containing Functional Groups on Multi-wall Carbon Nanotubes toward Supercapacitors. *Mater. Today Chem.* **2021**, *19*, 100414−100421.
(20) An, N.; Guo, Z.; Xin, J.; He, Y. Y.; Xie, K. F.; Sun, D. M.; Dong, X. Y.; Hu, Z. G. Hierarchical Porous Covalent Organic Framework/Graphene Composite Aerogel for High-Performance Supercapacitors. *J. Mater. Chem. A* **2021**, *9*, 16824−16833.
(21) Teimuri-Mofrad, R.; Hadi, R.; Abbasi, H.; Payami, E.; Neshad, S. Green Synthesis of Carbon Nanotubes@tetraferrocenylporphyrin/Copper Nanohybrid and Evaluation of Its Ability as a Supercapacitor. *J. Organomet. Chem.* **2019**, *899*, 120915−120923.
(22) Zhuang, X. D.; Zhao, W. X.; Zhang, F.; Cao, Y.; Liu, F.; Bia, S. A.; Feng, X. L. A Two-Dimensional Conjugated Polymer Framework with Fully sp^2-Bonded Carbon Skeleton. *Polym. Chem.* **2016**, *7*, 4176−4181.
(23) Torad, N. L.; Salunkhe, R. R.; Li, Y.; Hamoudi, H.; Imura, M.; Sakka, Y.; Hu, C. C.; Yamauchi, Y. Electric Bouble-Layer Capacitors Based on Highly Graphitized Nanoporous Carbons Derived from ZIF-67. *Chemistry* **2014**, *20*, 7895−7900.
(24) Chen, I. L.; Wei, Y. C.; Chen, T. Y.; Hu, C. C.; Lin, T. Oxidative Precipitation of Ruthenium Oxide for Supercapacitors: Enhanced Capacitive Performances by Adding Cetyltrimethylammonium Bromide. *J. Power Sources* **2014**, *268*, 430−438.
(25) Xue, R.; Guo, H.; Yue, L. G.; Wang, T.; Wang, M. Y.; Li, Q.; Liu, H.; Yang, W. Preparation and Energy Storage Application of a Long-Life and High Rate Performance Pseudocapacitive COF Material Linked with -NH-Bonds. *New J. Chem.* **2018**, *42*, 13726−13731.
(26) Vadiyar, M. M.; Liu, X. D.; Ye, Z. B. Macromolecular Polyethynylbenzonitrile Precursor-Based Porous Covalent Triazine Frameworks for Superior High-Rate High-Energy Supercapacitors. *ACS Appl. Mater. Interfaces* **2019**, *11*, 45805−45817.
(27) Geng, T. M.; Zhu, Z. M.; Zhang, W. Y.; Wang, Y. A Nitrogen-Rich Fluorescent conjugated Microporous Polymer with Triazine and Triphenylamine Units for High Iodine Capture and Nitro Aromatic Compound Detection. *J. Mater. Chem. A* **2017**, *5*, 7612−7617.
(28) Nishihara, H.; Hirota, T.; Matsuura, K.; Ohwada, M.; Hoshino, N.; Akutagawa, T.; Higuchi, T.; Jinnai, H.; Koseki, Y.; Kasai, H.; Matsuo, Y.; Maruyama, J.; Hayasaka, Y.; Konaka, H.; Yamada, Y.; Yamaguchi, S.; Kamiya, K.; Kamimura, T.; Nobukuni, H.; Tani, F. Synthesis of Ordered Carbonaceous Frameworks from Organic Crystals. *Nat. Commun.* **2017**, *8*, 109−118.
(29) Nishihara, H.; Matsuura, K.; Ohwada, M.; Yamamoto, M.; Matsuo, Y.; Maruyama, J.; Hayasaka, Y.; Yamaguchi, S.; Kamiya, K.; Konaka, H.; Inoue, M.; Tani, F. Synthesis of Ordered Carbonaceous Framework with Microporosity from Porphyrin with Ethynyl Groups. *Chem. Lett.* **2020**, *49*, 619−623.
(30) Ogoshi, T.; Sakatsume, Y.; Onishi, K.; Tang, R.; Takahashi, K.; Nishihara, H.; Nishina, Y.; Campéon, B. D. L.; Kakuta, T.; Yamagishi, T. The Carbonization of Aromatic Molecules with Three-Dimensional Structures Affords Carbon Materials with Controlled Pore Sizes at the Ångstrom-Leve. *Commun. Chem.* **2021**, *4*, 75−80.
(31) Chida, K.; Yoshii, T.; Takahashi, K.; Yamamoto, M.; Kanamaru, K.; Ohwada, M.; Deerattrakul, V.; Maruyama, J.; Kamiya, K.; Hayasaka, Y.; Inoue, M.; Tanig, F.; Nishihara, H. Force-Responsive Ordered Carbonaceous Frameworks Synthesized from Ni-Porphyrin. *Chem. Commun.* **2021**, *57*, 6007−6010.
(32) Xu, Y. J.; Wu, S. P.; Ren, S. J.; Ji, J. Y.; Yue, Y.; Shen, J. J. Nitrogen-Doped Porous Carbon Materials Generated via Conjugated Microporous Polymer Precursors for CO_2 Capture and Energy Storage. *RSC Adv.* **2017**, *7*, 32496−32501.
(33) Zhang, Y. N.; Mao, T. Y.; Wu, H.; Cheng, L. F.; Zheng, L. X. Carbon Nanotubes Grown on Flax Fabric as Hierarchical All-Carbon Fexible Electrodes for Supercapacitors. *Adv. Mater. Interfaces* **2017**, *4*, 1601123−1601129.
(34) Meng, J. S.; Niu, C. J.; Xu, L. H.; Li, J. T.; Liu, X.; Wang, X. P.; Wu, Y. Z.; Xu, X. M.; Chen, W. Y.; Li, Q.; Zhu, Z. Z.; Zhao, D. Y.; Mai, L. Q. General Oriented Formation of Carbon Nanotubes from Metal-Organic Frameworks. *J. Am. Chem. Soc.* **2017**, *139*, 8212−8221.
(35) Sevilla, M.; Yu, L. H.; Zhao, L.; Ania, C. O.; Titiricic, M. Surface Modification of CNTs with N-Doped Carbon: An Effective Way of Enhancing Their Performance in Supercapacitors. *ACS Sustainable Chem. Eng.* **2014**, *2*, 1049−1055.
(36) Wang, D. G.; Wang, H.; Lin, Y.; Yu, G. P.; Song, M.; Zhong, W. B.; Kuang, G. Synthesis and Morphology Evolution of Ultrahigh Content Nitrogen-Doped, Micropore-Dominated Carbon Materials as High-Performance Supercapacitors. *ChemSusChem* **2018**, *11*, 3932−3940.
(37) Zhao, Y. B.; Yuan, Y.; Xu, Y. M.; Zheng, G. Y.; Zhang, Q.; Jiang, Y. Q.; Wang, Z. Y.; Bu, N. S.; Xia, L. X.; Yan, Z. J. Fine-Regulating Ultramicropore of Porous Carbon via a Self-Sacrificial Template Route for High-Performance Supercapacitors. *Nanoscale* **2021**, *13*, 1961−1969.
(38) Zhang, C. G.; Meng, J.; Ma, K.; Jiao, X.; Yuan, Z. H. A Three-Dimensional Structure of Ternary Carbon for High Performance Supercapacitor. *Diamond Relat. Mater.* **2020**, *109*, 108075−108086.
(39) Li, Y. Q.; Roy, S.; Ben, T.; Xua, S. X.; Qiu, S. L. Micropore Engineering of Carbonized Porous Aromatic Framework (PAF-1) for Supercapacitors Application. *Phys. Chem. Chem. Phys.* **2014**, *16*, 12909−12917.
(40) Lv, Y. K.; Gan, L. H.; Liu, M. X.; Xiong, W.; Xu, Z. J.; Zhu, D. Z.; Wright, D. S. A Self-Template Synthesis of Hierarchical Porous Carbon Foams Based on Banana Peel for Supercapacitor Electrodes. *J. Power Sources* **2012**, *209*, 152−157.
(41) Abuzeid, H. R.; EL-Mahdy, A. F. M.; Ahmed, M. M. M.; Kuo, S. Triazine-Functionalized Covalent Benzoxazine Framework for Direct Synthesis of N-Doped Microporous Carbon. *Polym. Chem.* **2019**, *10*, 6010−6020.
(42) Jiang, Y.; Wang, Y.; Zeng, D. H.; Wang, Y.; Ma, Y. D.; Wang, H.; Zhang, X.; Dai, X. P. A Template-Assisted Strategy to Synthesize a Dilute CoNi Alloy Incorporated into Ultramicroporous Carbon for High Performance Supercapacitor Application. *Dalton Trans.* **2019**, *48*, 4702−4711.
(43) Zhao, Y. H.; Liu, M. X.; Gan, L. H.; Ma, X. M.; Zhu, D. Z.; Xu, Z. J.; Chen, L. W. Ultramicroporous Carbon Nanoparticles for the High-Performance Electrical Double-Layer Capacitor Electrode. *Energy Fuels* **2014**, *28*, 1561−1568.
(44) Liao, Y. Z.; Wang, H. G.; Zhu, M. F.; Thomas, A. Efficient Supercapacitor Energy Storage Using Conjugated Microporous Polymer Networks Synthesized from Buchwald-Hartwig Coupling. *Adv. Mater.* **2018**, *12*, 105701−1705710.

https://doi.org/10.1021/acs.inorgchem.1c02673
Inorg. Chem. 2021, 60, 18058−18064